How to cite: *Angew. Chem. Int. Ed.* **2022,** *61,* e202207013
International Edition: doi.org/10.1002/anie.202207013
German Edition: doi.org/10.1002/ange.202207013

Nitride Nanocrystal Synthesis

The Chemistry of Cu_3N and Cu_3PdN Nanocrystals**

*Mahsa Parvizian, Alejandra Duràn Balsa, Rohan Pokratath, Curran Kalha, Seungho Lee, Dietger Van den Eynden, Maria Ibáñez, Anna Regoutz, and Jonathan De Roo**

Abstract: The precursor conversion chemistry and surface chemistry of Cu_3N and Cu_3PdN nanocrystals are unknown or contested. Here, we first obtain phase-pure, colloidally stable nanocubes. Second, we elucidate the pathway by which copper(II) nitrate and oleylamine form Cu_3N. We find that oleylamine is both a reductant and a nitrogen source. Oleylamine is oxidized by nitrate to a primary aldimine, which reacts further with excess oleylamine to a secondary aldimine, eliminating ammonia. Ammonia reacts with Cu^I to form Cu_3N. Third, we investigated the surface chemistry and find a mixed ligand shell of aliphatic amines and carboxylates (formed in situ). While the carboxylates appear tightly bound, the amines are easily desorbed from the surface. Finally, we show that doping with palladium decreases the band gap and the material becomes semi-metallic. These results bring insight into the chemistry of metal nitrides and might help the development of other metal nitride nanocrystals.

Introduction

Metal nitrides are a versatile class of materials with increasing interest.[1] Copper nitride (Cu_3N) specifically has garnered attention as an inexpensive, non-toxic material with potential applications in solar cells,[2] high-density optical data storage,[3] and electrocatalysis (oxygen evolution and CO_2 reduction).[4] Cu_3N is a semiconductor with a calculated indirect band gap of 1 eV and an anti-ReO_3 cubic crystal structure.[2,5] The body center position can be occupied by dopants (e.g., palladium) forming structures such as Cu_3Pd_xN. Upon doping, the lattice constant increases,[6] and the electronic structure of the material is reported to change from semiconducting to semi-metallic.[7]

Bulk Cu_3N forms at relatively low temperature but decomposes at higher temperature (475 °C) to metallic copper (under inert atmosphere) or copper oxide (in air).[3,8] The first wet-chemical synthesis of bulk Cu_3N powders were based on aminolysis or the solvothermal decomposition of copper azides.[8,9] Ultra-small (2–4 nm) and colloidally stable nanocrystals of Cu_3N have been synthesized from $Cu(OMe)_2$ in benzylamine[10] or by aminolysis of Cu^I in pyridine.[11] Larger colloidal Cu_3N nanocubes have been obtained from copper nitrate and alkylamine (Scheme 1).[4a,c,12] In most cases, additional solvent is added (usually 1-octadecene, ODE). The equivalents of ligand (32–66), the reaction temperature (220–280 °C), and time (10–60 min) vary, as does the nature of the alkyl chain of the amine (oleylamine, hexadecylamine or octadecylamine). Changing the nature of the amine allows to tune the final size from 10 to 25 nm.[12a]

Unfortunately, the reaction mechanism and the by-products are not well established. Some authors claim that nitrate is the nitrogen source, and thus nitrogen is supposed to be reduced from its highest oxidation state in nitrate to its lowest oxidation state in nitride, and this process is presumably catalyzed by the amine ligand.[12c] Such an eight-electron redox process is unlikely to happen in a single reaction. Other authors assume that Cu^{II} is first fully reduced to Cu^0 and subsequently reacts with dinitrogen (a possible decomposition product of the nitrate complex).[13] However, the nitrogen-nitrogen bond in dinitrogen is extremely strong (946 kJ mol^{-1}),[14] and N_2 is thus not likely to react with elemental copper at 250 °C. There is currently insufficient evidence to claim a mechanism for the precursor conversion. Regarding the crystallization mechanism, it was shown that first small, amorphous particles form, which subsequently ripen into Cu_3N nanocubes.[4c]

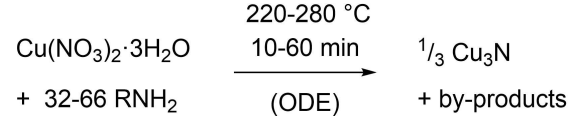

Scheme 1. The range of conditions reported for the synthesis of colloidal Cu_3N nanocrystals.

[*] M. Parvizian, A. Duràn Balsa, R. Pokratath, D. Van den Eynden, J. De Roo
Department of Chemistry, University of Basel
4058 Basel (Switzerland)
E-mail: jonathan.deroo@unibas.ch
C. Kalha, A. Regoutz
Department of Chemistry, University College London
20 Gordon Street, London, WC1H 0AJ (UK)
S. Lee, M. Ibáñez
IST Austria
Am Campus 1, 3400 Klosterneuburg (Austria)

[**] A previous version of this manuscript has been deposited on a preprint server (https://doi.org/10.26434/chemrxiv-2022-2tjc0-v2).

The surface chemistry of Cu_3N nanocrystals is also unknown. Although alkylamines are the only ligand present during the synthesis, there are several examples where the ligands can convert to other ligands during nanocrystal synthesis, leading to surprising surface chemistries.[15] Given the importance of surface chemistry for nanocrystal applications it is imperative to elucidate and control it.[16] Amines typically bind to the nanocrystal surface as Lewis basic (L-type) ligands and feature an adsorption–desorption equilibrium that is often highly dynamic.[17] However, in the case of copper-based nanocrystals, amines have been observed to be tightly bound.[18] It is thus surprising that Cu_3N nanocrystals have generally poor colloidal stability after purification.

In this work, we aimed at elucidating the precursor conversion mechanism and surface chemistry of Cu_3N (and Cu_3PdN) nanocrystals, synthesized from copper nitrate (and palladium acetylacetonate). We first screened the different synthetic methods in the literature, and found the report of Vaughn et al. as the most reproducible.[12b,19] We then explored the influence of different parameters on the reaction outcome, including the presence of water, temperature, time, etc. Having obtained the optimal conditions to form phase pure Cu_3N nanocubes, we then redesigned the purification procedure to yield colloidally stable Cu_3N nanocrystals. We uncovered the precursor conversion mechanism of the reaction. We found that nitrate and Cu^{II} both oxidize alkylamine to a primary aldimine, forming also Cu^{I}. Condensation of the primary aldimine with a second equivalent alkylamine, yields a secondary aldimine and ammonia. The latter is the active nitrogen precursor and reacts with Cu^{I} to Cu_3N. Finally, the surface of these Cu_3N and Cu_3PdN particles has been analyzed. X-ray photoelectron spectroscopy (XPS) and Fourier Transform Infrared spectroscopy (FTIR) established the presence of carboxylate ligands on the surface, together with amine ligands. Advanced nuclear magnetic resonance (NMR) spectroscopy revealed the dynamics of ligands binding. These fundamental chemistry insights will enable the elucidation of formation mechanisms of other copper-based colloidal nanocrystals and other metal nitrides.

Results and Discussion

We decided to optimize the procedure reported by Vaughn et al. by exploring the influence of different parameters.[12b] First, we replaced 1-octadecene (the solvent) with hexadecane since we reported earlier that 1-octadecene polymerizes at 240 °C, contaminating the final nanocrystal product and complicating the purification.[20] Concerning reaction temperature, crystalline Cu_3N was formed between 220 °C and 260 °C (after 15 minutes), with the highest crystallinity for 260 °C (Figure S1). Interestingly, the crystallite size was found to be quite independent of the reaction temperature; 10–11 nm according to the Scherrer analysis of the powder XRD (X-ray diffraction) reflections. At 200 °C, no particles could be isolated. Furthermore, we took reaction aliquots at 5, 10, 15, 30, and 60 min at 240 °C and 260 °C. Each aliquot was purified and analyzed by transmission electron microscopy (TEM) to observe the nanocrystal growth throughout the reaction. At 240 °C, we observed both small dots and fully formed nanocubes up to 15 min of reaction time (Figures S2). The small particles presumably ripen in the bigger nanocubes since the former disappear at 30 min. After 60 minutes at 240 °C, the XRD showed pure Cu_3N. By comparison, at 260 °C, the nanocubes were already fully formed after 15 min. After 30 min at 260 °C, the particles started to decompose and crystalline Cu^0 was formed. Some Cu_2O could also be detected as a minority phase after full decomposition. (Figure S3).

The reported procedure has two steps where vacuum is applied. This leads us to investigate the role of water and whether an inert atmosphere is strictly necessary. Note that the precursor contains water (an equivalent of 13 μL for a standard synthesis). We obtained identical Cu_3N nanocrystals when the vacuum steps were omitted, or, when after applying vacuum (presumably removing water), 13 μL of water was injected into the reaction mixture (Figures S4, S5). However, the same reaction in an open flask did not yield Cu_3N (or any isolatable material), indicating that an important gaseous intermediate can escape from the reaction mixture. To work under controlled and reproducible conditions, we still choose to perform a short (30 min) degassing step at 50 °C, but it appears that the synthesis is robust against air or water contamination. We also found that both 30 and 60 equivalents of amine ligands yielded Cu_3N nanocrystals (Figure S6). Based on the above optimization, we arrived at the conditions in Scheme 2.

After applying the reported precipitation-and-redispersion cycles (with ethanol and toluene),[12b] the particles were redispersed in toluene (5 mL), but they precipitated within a couple of minutes, see Figure 1. Since the nanocrystals were colloidally stable in the crude reaction mixture, we hypothesized that the ligands desorbed from the surface during the precipitation-and-redispersion cycles. The nature and volume of the solvent used for redispersion play an important role since they determine the position of the adsorption–

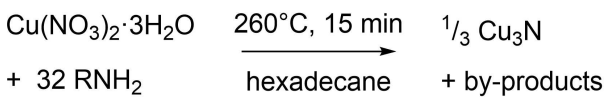

Scheme 2. The conditions that lead most reproducibly to phase-pure Cu_3N nanocrystals.

Figure 1. Photograph of Cu_3N nanocrystals after regular (left) and optimized (right) purification.

desorption equilibrium. The ligand–solvent interaction should be favorable enough to disperse the nanocrystals, but not so high that ligands prefer to be fully solvated over being bound to the surface.[21] During purification, it is also preferred to work with quite concentrated dispersions to minimize the loss of nanocrystals over several cycles. On the other hand, too high concentrations might cause impurities to be trapped between the flocculating nanocrystals. Considering the above points, we adapted the purification procedure. Various solvents (toluene, hexane, chloroform, and cyclohexane), as well as non-solvents (acetone, ethanol, and methanol), were tested. Our final procedure involves two precipitation cycles with acetone (15 mL) followed by a final precipitation with ethanol (15 mL), always redispersing in cyclohexane (5 mL).[22] A 10 v% solution of distilled oleylamine was added after the first acetone wash (1 mL) and after the second acetone wash (2 mL) followed by 5 minutes of sonication. There was no need for a final oleylamine addition after the ethanol wash and the nanocrystals remained colloidally stable. This procedure thus minimized the amount of excess ligand in the final product but provided a stable dispersion (11 mg mL^{-1}) of oleylamine-capped Cu_3N nanocrystals (Figure 1). From thermogravimetric analysis (TGA), we determined that the dried samples contained 29.2 w % organics (ligands) and the final Cu_3N yield is 96 % (Figure S7).

Copper palladium nitride (Cu_3PdN) nanocrystals were also synthesized. The procedure was identical to that of Cu_3N, except for the reaction temperature (240 °C) and the addition of 0.33 equivalents of palladium(II) acetylacetonate, alongside the $Cu(NO_3)_2$. The doped nanocrystals were purified with the optimized purification method. The synthesis yielded black nanoparticles that were colloidally stable (13 mg mL^{-1}). According to TGA, ligands make up 13.22 w% of the dried mass (assuming perfect Cu_3PdN stoichiometry) and the Cu_3PdN yield is 91 % (Figure S7).

The final dispersions of Cu_3N and Cu_3PdN nanocrystals were analyzed with TEM, XRD and dynamic light scattering (DLS) (Figure 2). According to TEM, the average cube edge length is 13.5 nm ($\sigma = 1.9$ nm) for the Cu_3N nanocubes and 10.2 nm ($\sigma = 1.4$ nm) for the Cu_3PdN nanocrystals. The solvodynamic diameter obtained from DLS analysis were 17 nm for Cu_3N and 13 nm for Cu_3PdN. The sizes obtained via DLS are in line with the sizes obtained via TEM since DLS determines the solvodynamic size of the whole particle, including the surface ligands. Both TEM and DLS support that the dispersions are highly stable since no aggregates are observed. XRD shows quite sharp reflections for Cu_3N (crystallite size = 9.0 ± 1.7 nm), while they are broader for Cu_3PdN (crystallite size = 4.5 ± 1.1 nm). Compared with the sizes obtained from TEM, it is clear that the Cu_3PdN nanocrystals are polycrystalline. A real space refinement of the Pair Distribution Function further confirms the structure of Cu_3N and Cu_3PdN (Figure S8).

Regarding the precursor conversion mechanism, we found the proposed pathways in literature implausible and therefore proposed an alternative hypothesis in which the active nitride source is ammonia, see Scheme 3. First, oleylamine is oxidized to a primary aldimine by nitrate.

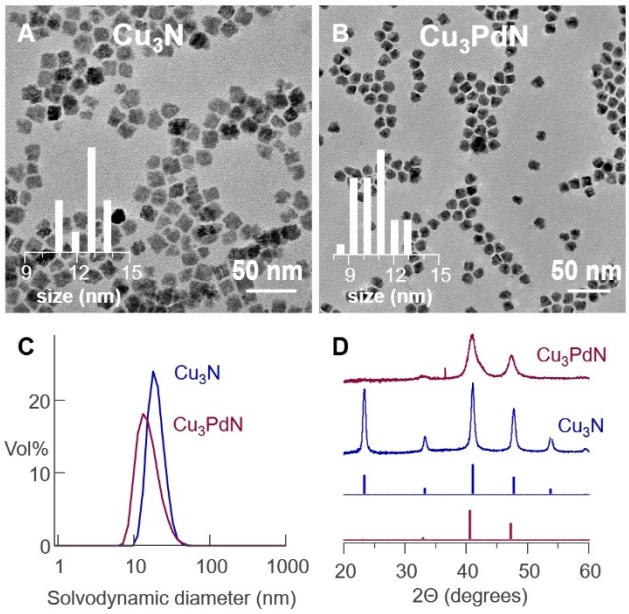

Figure 2. TEM images of A) Cu_3N and B) Cu_3PdN. The histograms are shown as an inset. The cube edge length is used as a measure for size. C) DLS and D) powder XRD measurements (the reference XRD reflections are shown as well).

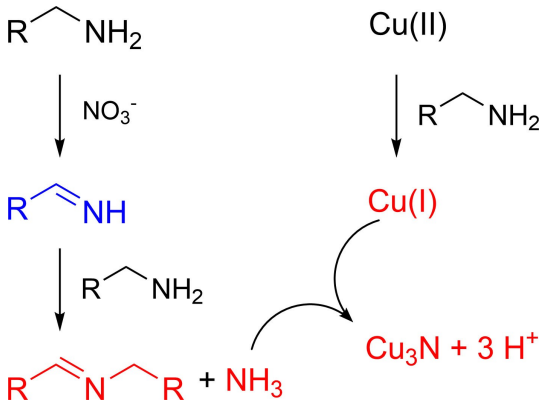

Scheme 3. Our proposed pathway for Cu_3N formation. Precursors are shown in black, detected species in red, and hypothesized intermediates in blue.

Nucleophilic addition of a second equivalent of oleylamine forms the more stable, secondary aldimine with the elimination of ammonia. Ammonia reacts with Cu^I to Cu_3N, releasing three protons. The Cu^I species was generated by reduction of Cu^{II} by oleylamine upon heating. Cyclic voltammetry confirms a lower reduction potential of Cu^{II} to Cu^I upon addition of oleylamine (at room temperature).[23] We hypothesize that the co-product of this Cu^{II} reduction is the same primary aldimine as mentioned before.

The copper precursor, $Cu(NO_3)_2{\cdot}3H_2O$, does not dissolve in the solvent (hexadecane) until oleylamine is added, indicating the formation of a coordination complex. This is supported by the deep blue color of the reaction mixture, typical for Cu^{II} coordinated by amines.[24] During the heat-

up to 260 °C, the color of the solution changes from blue to yellow around 185 °C, indicating the reduction of Cu^{II} to Cu^{I}. Concomitant with the color change, new resonances appear in the ^{1}H NMR spectrum of the reaction mixture (Figure 3). We assign these resonances to the secondary aldimine. Upon reaching the reaction temperature (240–260 °C), the reaction mixture turns brown (indicating the formation of Cu_3N), and we observe in the ^{1}H NMR spectrum a significant increase in the aldimine concentration (Figure 3). We confirmed the identity of the aldimine by synthesizing the secondary aldimine of dodecyl aldehyde and octadeylamine, and we found perfect agreement of the resonances **1**–**3**.

Ammonia is detected in the reaction mixture by bubbling Ar through the reaction mixture during synthesis, and dissolving the gasses in either 40 mL or 80 mL water. A commercial ammonia test kit indicates a concentration of 200 mg L^{-1} or 100 mg L^{-1} respectively (Figure S9). Given that the reaction is executed at a scale of 0.24 mmol Cu, and assuming that every nitrate (0.48 mmol) oxidizes one oleylamine molecule, this is the expected amount of ammonia (0.48 mmol, 8 mg). We can also quantify the aldimine formation by using the alkene resonance of oleylamine as the internal standard. For every aldimine, we find 18 oleyl chains, indicating a conversion of 5.5 %. Given that 7.6 mmol oleylamine was used, this amounts to 0.42 mmol aldimine. This value is in reasonable agreement with the amount of ammonia detected (taking into account the error on the ammonia measurement and the fact that oleylamine is only 70 % pure). This quantitative picture thus confirms our hypothesis and indicates a one-to-one stoichiometry between nitrate, aldimine, and ammonia. We did not obtain Cu_3N in this experiment since we removed ammonia from the reaction mixture. This indicates that ammonia is essential in nitride formation. Literature shows that ammonia indeed reacts with copper salts to Cu_3N.[11,25]

We also quantified the small amount of aldimine (0.1 mmol) generated during the reduction of Cu^{II} to Cu^{I}. This value is about half of the copper amount (0.24 mmol) and can be easily rationalized based on electron counting in the redox reactions. Indeed, the reduction of Cu^{II} to Cu^{I} is a one-electron process while the oxidation of primary amine to aldimine is a two-electron process (Scheme 4). Aldimine has also been observed in the synthesis of Cu^0 and Pd^0 nanocrystals,[26] and it appears to be the typical oxidation product of oleylamine. Scheme 4 also makes clear that the oxidation of primary amine generates a large amount of protons which are presumably absorbed by the excess oleylamine. These protons are observed in the ^{1}H NMR spectrum as a broad resonance around 3 ppm (see Figure 3). They do not appear in the typical region for alkylammonium resonances, since maximally 1.2 mmol protons are generated and oleylamine is still present in excess (7 mmol). Given that proton equilibria are typically fast, we thus observe the population averaged chemical shift between protonated oleylamine and unprotonated oleylamine.

Our proposed pathway requires a primary amine. To further test our hypothesis, we thus attempted the synthesis of Cu_3N with dioctylamine and trioctylamine. As expected, the reaction did not produce Cu_3N but Cu_2O instead (Figure 4). Also in the NMR spectrum, we do not find aldimine in the case of trioctylamine and only a very small amount in the case of dioctylamine. The latter can be

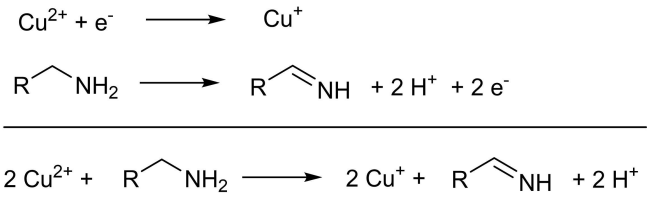

Scheme 4. Redox half reactions and overall reaction for the reduction of Cu^{2+} by primary amines.

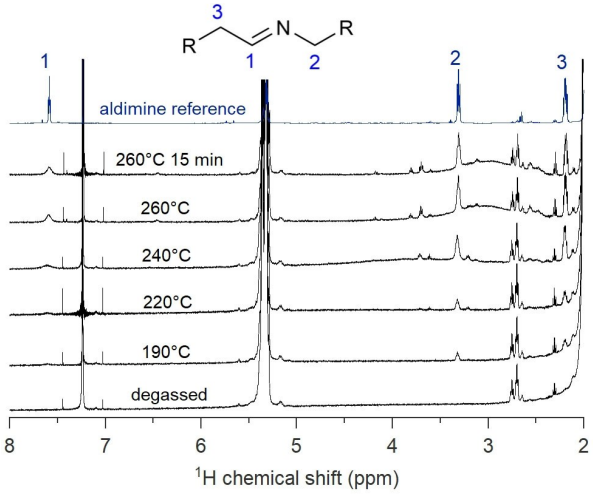

Figure 3. ^{1}H NMR spectra of aliquots after degassing, at 190 °C (after the color change), at 220 °C, at 240 °C, at 260 °C and at the end of the reaction. Aldimine formation is observed starting from 190 °C. The aldimine reference is shown for comparison.

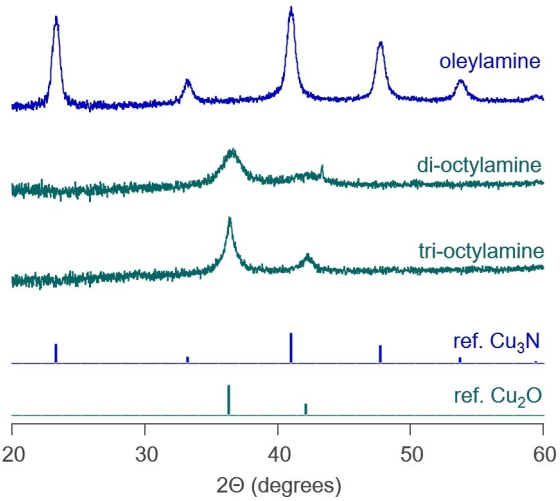

Figure 4. XRD spectra of the syntheses with different amines. The reference of bulk Cu_3N (blue) and bulk Cu_2O (green) are shown.

directly oxidized to a secondary aldimine, without a primary aldimine intermediate (and thus without ammonia elimination) (Figure S10). As an additional control, we performed a reaction with copper nitrate and dioctylamine, and bubbled ammonia through the reaction mixture as soon as Cu^{I} is formed. XRD analysis shows that Cu_3N is formed during this reaction along with some Cu_2O (Figure S11). This control experiment suggests that our proposed pathway—Cu^{I} reacting with in situ produced ammonia—is plausible.

We thus firmly established that nitrate is not the nitrogen source for Cu_3N but rather oxidizes the amine to aldimine. Cu_3PdN nanocrystals follows the same mechanism based on the formation of aldimine and ammonia during the reaction (Figure S12). The mechanism is reminiscent of the one for InN, where In^{3+} oxidizes primary amines into aldimine and nucleophilic attack of lithium oleylamide generates amide, NH_2^-.[27] However, an important difference is that for copper, an additional oxidant (nitrate) is required. The reduction of Cu^{2+} alone does not seem to generate sufficient ammonia to form copper nitride since other copper salts do not generate copper nitride.[12c] Or perhaps it generates ammonia at too low temperatures, where the formation of Cu_3N is not yet favored. More detailed insight into the crystallization mechanism of Cu_3N could shed light on this issue.

X-ray photoelectron spectroscopy (XPS) was used to explore the surface chemistry. Survey spectra for both compounds (Figure S13) show spectral signatures from all expected elements. In addition, a small amount of Si was detected most likely from the silicone grease used during the synthesis. The binding energy (BE) position of the main feature in the Cu $2p_{3/2}$ core level (932.7 ± 0.1 eV) is commensurate with the expected Cu^{I} oxidation state for both samples (Figure 5A). In addition, both samples show a shoulder towards the higher BE of the main peak (marked with an asterisk in Figure 5A) and in the Cu_3PdN sample, a clear Cu^{II} satellite is also visible. From peak fit analysis (Figure S14), the contribution of these additional chemical states relative to the main Cu^{I} line is 12.3 ± 0.5 rel. at.% for Cu_3N and 17.9 ± 0.5 rel.at.% for Cu_3PdN, respectively. The Pd $3d$ core level (Figure 5B) is only observed for the Cu_3PdN sample. The BE of the Pd $3d_{5/2}$ component (335.5 ± 0.1 eV) is commensurate with Pd^0 or Pd^{I} with a spin-orbit-splitting of the doublet of 14.6 eV. In both samples, the N $1s$ core level (Figure 5C) displays two contributions. The lower BE feature at 397.8 ± 0.2 eV corresponds to metal-nitride and the higher BE feature at 399.6 ± 0.2 eV corresponds to the expected oleylamine ligand, bound to the nanocrystal surface. The O $1s$ core level (Figure 5D) shows three discernible contributions from metal oxide, metal hydroxide, and carboxylate environments. Together with the Cu^{II} species, we infer that the surface of the particles contains an amorphous copper oxyhydroxide layer. The carboxylate is assigned to a surface bound oleate ligand and its presence is also detected by FTIR (broad signal at 1577 cm^{-1}, see Figure S15). Oleate is most likely formed by oxidation of oleylamine by nitrate, as we reported earlier in the synthesis of cerium oxide nanocrystals.[15b]

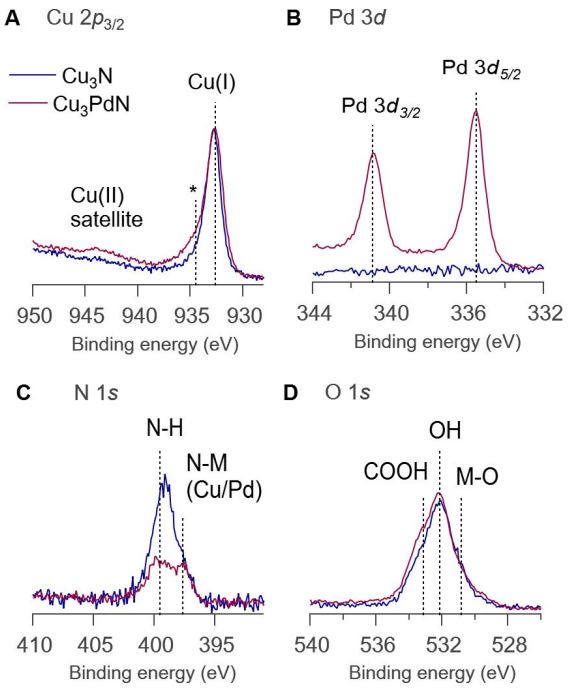

Figure 5. XPS core level spectra of Cu_3N and Cu_3PdN, including A) Cu $2p_{3/2}$, B) Pd $3d$, C) N $1s$, and D) O $1s$.

The ^1H NMR spectra of Cu_3N and Cu_3PdN show the typical signature of an oleyl chain (Figure 6A). While the alkene resonance is reasonably sharp, the resonances close to the binding group are indistinguishable from the background. This broadening is likely due to fast T_2 relaxation induced by copper.[18b] Based on the line width of the alkene resonance,[28] we inferred that the ligand is dynamic and in fast exchange between a bound and free state. This is confirmed by a relatively high diffusion coefficient ($D = 174\ \mu m^2 s^{-1}$) determined by pulsed field gradient experiments on the Cu_3N dispersion (Figure S16). For Cu_3PdN, we noticed a second, very broad alkene resonance of low intensity underneath the sharp signal. A careful pulsed field gradient experiment revealed that the alkene resonance is a superposition of two species, one diffusing with $D = 48\ \mu m^2 s^{-1}$ and the other one with $D = 667\ \mu m^2 s^{-1}$ (Figure 6 B). The small diffusion coefficient corresponds to a solvodynamic diameter of 17 nm (via the Stokes–Einstein equation), which agrees quite well with a nanocrystal of 12 nm and a ligand shell of 2 nm thickness. We thus assign the broad resonance to tightly bound ligand, presumably the oleate. The larger diffusion constant corresponds most likely to oleylamine. We could only detect the tightly bound oleate in the Cu_3PdN sample, but oleate is also present on the surface of Cu_3N according to our XPS results, albeit to a lesser extent. Unfortunately, all NMR signals appear more broadened in the Cu_3N sample and the tightly bound oleate could not be detected in NMR.

In addition to the identification of the chemical species present in the samples, XPS was also used to probe the electronic structure of Cu_3N and Cu_3PdN by collecting valence band spectra. Figure 7A shows the valence band

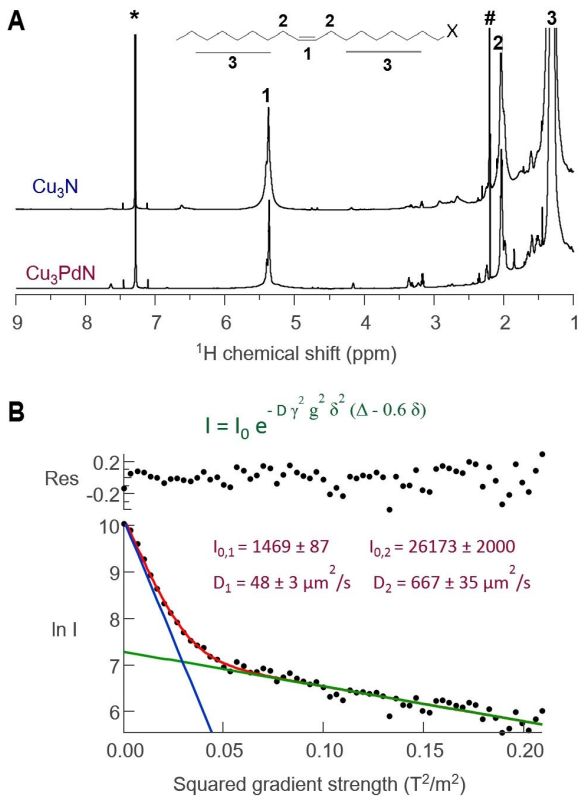

Figure 6. Nuclear magnetic resonance spectroscopy of the purified Cu_3N and Cu_3PdN NCs. A) ^1H NMR spectrum in chloroform-*d* of the NCs indicating the presence of an oleyl chain. B) Diffusion decay of the alkene region of the Cu_3PdN NCs showing a slow and a fast diffusing species. The residuals of the fit are also shown.

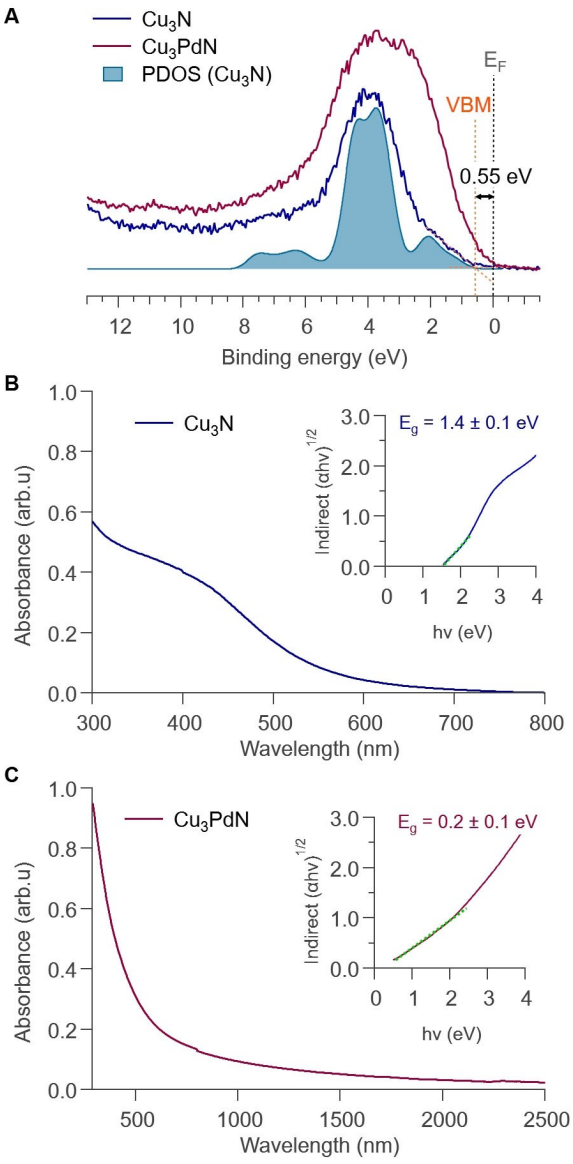

Figure 7. A) Valence region of Cu_3N and Cu_3PdN, including XPS valence spectra and the broadened and cross-section-weighted sum of the projected density of states (PDOS) from density functional theory (DFT). The position of the valence band maximum (VBM) of Cu_3N and the position of the Fermi energy (E_F) are also shown. B), C) UV/Vis absorption spectra of Cu_3N in cyclohexane and Cu_3PdN in tetrachloroethylene with their corresponding Tauc plots as an inset, respectively. Indirect band gaps were determined from linear fitting to the low energy region of the Tauc plots (shown in dotted green line).

spectra of the two compounds, as well as the broadened and cross section weighted total density of states of Cu_3N from density functional theory (DFT) calculations. The experimental and theoretical results for Cu_3N agree very well. The projected density of states calculations (Figure S17) show that the valence band of Cu_3N is dominated by Cu 3*d* states with only minor mixing of Cu 3*p* states and minimal nitrogen contributions. The valence band maximum (VBM) position of Cu_3N is 0.55 ± 0.05 eV from the Fermi energy E_F. In comparison, the valence spectrum of Cu_3PdN shows additional intensity towards the E_F from Pd states closing the VBM-E_F gap. In parallel, UV/Vis has been used to determine the optical band gap of the particles. An indirect band gap has been reported for Cu_3N thin films according to theoretical band structure calculations.[2] To our knowledge, the type of optical band gap (direct or indirect) has not yet been reported for Cu_3PdN. In this work, we assumed an indirect optical band gap for both samples. A Tauc plot analysis resulted in an optical band gap of 1.4 ± 0.1 eV and 0.2 ± 0.1 eV for our Cu_3N and Cu_3PdN NCs, respectively (Figure 7B and C). The reduction in optical band gap is commensurate with the closing of the electronic VBM-E_F separation observed in XPS.

Conclusion

In conclusion, we successfully optimized the synthesis of Cu_3N and Cu_3PdN nanocrystals in order to obtain phase pure, colloidally stable nanocrystals via modulating the reaction parameters with a focus on the purification. We provided experimental support for a precursor conversion pathway that hypothesized ammonia as the active nitrogen

source. We proposed that primary aldimine is the oxidation product of the ligand (oleylamine), oxidized by both Cu^{II}, and nitrate. Nucleophilic addition and elimination of a second oleylamine molecule onto the primary aldimine released ammonia, which subsequently reacted with Cu^{I} to form Cu_3N and Cu_3PdN. The surface of the nanocrystals was capped by a mixture of oleylamine and oleate. The latter was formed in situ from the further oxidation of aldimine. The addition of palladium to copper nitride reduces the optical band gap as well as the separation between the valence band maximum (VBM) and Fermi energy E_F.

Acknowledgements

J.D.R. and M.P. acknowledge the SNF Eccellenza funding scheme (project number: 194172). We acknowledge DESY (Hamburg, Germany), a member of the Helmholtz Association HGF, for the provision of experimental facilities. Parts of this research were carried out at beamline P21.1, PETRA III. We thank Dr. Soham Banerjee for acquiring the PDF data and helpful advice. A.R. acknowledges the support from the Analytical Chemistry Trust Fund for her CAMS-UK Fellowship. C.K. acknowledges the support from the Department of Chemistry, UCL. The authors acknowledge Dr Stephan Lany from NREL for providing the Cu_3N DFT calculations. The authors thank Prof. Raymond Schaak and Dr. Robert William Lord for helpful advice and suggestions regarding the purification procedure. Open access funding provided by Universitat Basel.

Conflict of Interest

The authors declare no conflict of interest.

Data Availability Statement

The data that support the findings of this study are openly available in Zenodo at https://doi.org/10.5281/zenodo.6542908.

Keywords: Copper Nitride · Ligands · Nitrides · Reaction Mechanisms · Structural Analysis · Surface Chemistry

[1] a) Z. Chen, C. Sun, W. Guo, Z. Chen in *Nonmagnetic and Magnetic Quantum Dots* (Ed.: V. N. Stavrou), IntechOpen, Rijeka, **2017**; b) Y. Ma, L. Xiong, Y. Lu, W. Zhu, H. Zhao, Y. Yang, L. Mao, L. Yang, *Front. Chem.* **2021**, *9*, 638216; c) M. Parvizian, J. De Roo, *Nanoscale* **2021**, *13*, 18865–18882.

[2] A. Zakutayev, C. M. Caskey, A. N. Fioretti, D. S. Ginley, J. Vidal, V. Stevanovic, E. Tea, S. Lany, *J. Phys. Chem. Lett.* **2014**, *5*, 1117–1125.

[3] T. Maruyama, T. Morishita, *Appl. Phys. Lett.* **1996**, *69*, 890–891.

[4] a) Z. Yin, C. Yu, Z. Zhao, X. Guo, M. Shen, N. Li, M. Muzzio, J. Li, H. Liu, H. Lin, J. Yin, G. Lu, D. Su, S. Sun, *Nano Lett.* **2019**, *19*, 8658–8663; b) C. Panda, P. W. Menezes, M. Zheng, S. Orthmann, M. Driess, *ACS Energy Lett.* **2019**, *4*, 747–754; c) P. X. Xi, Z. H. Xu, D. Q. Gao, F. J. Chen, D. S. Xue, C. L. Tao, Z. N. Chen, *RSC Adv.* **2014**, *4*, 14206–14209.

[5] a) D. Bocharov, A. Anspoks, J. Timoshenko, A. Kalinko, M. Krack, A. Kuzmin, *Radiat. Phys. Chem.* **2020**, *175*, 108100–108104; b) G. Paniconi, Z. Stoeva, H. Doberstein, R. I. Smith, B. L. Gallagher, D. H. Gregory, *Solid State Sci.* **2007**, *9*, 907–913.

[6] a) X. Y. Cui, A. Soon, A. E. Phillips, R. K. Zheng, Z. W. Liu, B. Delley, S. P. Ringer, C. Stampfl, *J. Magn. Magn. Mater.* **2012**, *324*, 3138–3143; b) H. Jacobs, U. Zachwieja, *J. Less-Common Met.* **1991**, *170*, 185–190.

[7] a) U. Hahn, W. Weber, *Phys. Rev. B* **1996**, *53*, 12684–12693; b) F. Gulo, A. Simon, J. Kohler, R. K. Kremer, *Angew. Chem. Int. Ed.* **2004**, *43*, 2032–2034; *Angew. Chem.* **2004**, *116*, 2066–2068.

[8] J. Choi, E. G. Gillan, *Inorg. Chem.* **2005**, *44*, 7385–7393.

[9] a) U. Zachwieja, H. Jacobs, *J. Less-Common Met.* **1990**, *161*, 175–184; b) R. Juza, H. Hahn, *Z. Anorg. Allg. Chem.* **1939**, *241*, 172–178.

[10] R. Deshmukh, G. B. Zeng, E. Tervoort, M. Staniuk, D. Wood, M. Niederberger, *Chem. Mater.* **2015**, *27*, 8282–8288.

[11] A. Egeberg, L. Warmuth, S. Riegsinger, D. Gerthsen, C. Feldmann, *Chem. Commun.* **2018**, *54*, 9957–9960.

[12] a) H. Wu, W. Chen, *J. Am. Chem. Soc.* **2011**, *133*, 15236–15239; b) D. D. Vaughn Ii, J. Araujo, P. Meduri, J. F. Callejas, M. A. Hickner, R. E. Schaak, *Chem. Mater.* **2014**, *26*, 6226–6232; c) D. Wang, Y. Li, *Chem. Commun.* **2011**, *47*, 3604–3606; d) R. K. Sithole, L. F. E. Machogo, M. J. Moloto, S. S. Gqoba, K. P. Mubiayi, J. Van Wyk, N. Moloto, *J. Photochem. Photobiol. A* **2020**, *397*, 112577–112587.

[13] R. Kadzutu-Sithole, L. F. E. Machogo-Phao, T. Kolokoto, M. Zimuwandeyi, S. S. Gqoba, K. P. Mubiayi, M. J. Moloto, J. Van Wyk, N. Moloto, *RSC Adv.* **2020**, *10*, 34231–34246.

[14] C. E. Housecroft, A. G. Sharpe, *Inorganic Chemistry, 5th ed.*, Pearson, Upper Saddle River, **2018**.

[15] a) K. De Keukeleere, S. Coucke, E. De Canck, P. Van Der Voort, F. Delpech, Y. Coppel, Z. Hens, I. Van Driessche, J. S. Owen, J. De Roo, *Chem. Mater.* **2017**, *29*, 10233–10242; b) M. Calcabrini, D. Van den Eynden, S. S. Ribot, R. Pokratath, J. Llorca, J. De Roo, M. Ibanez, *JACS Au* **2021**, *1*, 1898–1903.

[16] M. A. Boles, D. Ling, T. Hyeon, D. V. Talapin, *Nat. Mater.* **2016**, *15*, 141–153.

[17] a) B. Fritzinger, I. Moreels, P. Lommens, R. Koole, Z. Hens, J. C. Martins, *J. Am. Chem. Soc.* **2009**, *131*, 3024–3032; b) N. C. Anderson, P. E. Chen, A. K. Buckley, J. De Roo, J. S. Owen, *J. Am. Chem. Soc.* **2018**, *140*, 7199–7205; c) C. Grote, K. J. Chiad, D. Vollmer, G. Garnweitner, *Chem. Commun.* **2012**, *48*, 1464–1466.

[18] a) R. Dierick, F. Van den Broeck, K. De Nolf, Q. Zhao, A. Vantomme, J. C. Martins, Z. Hens, *Chem. Mater.* **2014**, *26*, 5950–5957; b) A. Oliva-Puigdomènech, J. De Roo, J. Kuhs, C. Detavernier, J. C. Martins, Z. Hens, *Chem. Mater.* **2019**, *31*, 2058–2067.

[19] R. W. Lord, C. F. Holder, J. L. Fenton, R. E. Schaak, *Chem. Mater.* **2019**, *31*, 4605–4613.

[20] E. Dhaene, J. Billet, E. Bennett, I. Van Driessche, J. De Roo, *Nano Lett.* **2019**, *19*, 7411–7417.

[21] J. Zito, I. Infante, *Acc. Chem. Res.* **2021**, *54*, 1555–1564.

[22] D. Doblas, T. Kister, M. Cano-Bonilla, L. Gonzalez-Garcia, T. Kraus, *Nano Lett.* **2019**, *19*, 5246–5252.

[23] L. Castilla-Amorós, D. Stoian, J. R. Pankhurst, S. B. Varandili, R. Buonsanti, *J. Am. Chem. Soc.* **2020**, *142*, 19283–19290.

[24] a) F. Cui, Y. Yu, L. Dou, J. Sun, Q. Yang, C. Schildknecht, K. Schierle-Arndt, P. Yang, *Nano Lett.* **2015**, *15*, 7610–7615; b) S.

Jeong, Y. Liu, Y. Zhong, X. Zhan, Y. Li, Y. Wang, P. M. Cha, J. Chen, X. Ye, *Nano Lett.* **2020**, *20*, 7263–7271.
[25] T. Nakamura, H. Hayashi, T. A. Hanaoka, T. Ebina, *Inorg. Chem.* **2014**, *53*, 710–715.
[26] a) R. W. Man, A. R. Brown, M. O. Wolf, *Angew. Chem. Int. Ed.* **2012**, *51*, 11350–11353; *Angew. Chem.* **2012**, *124*, 11512–11515; b) F. Yarur Villanueva, P. B. Green, C. Qiu, S. R. Ullah, K. Buenviaje, J. Y. Howe, M. B. Majewski, M. W. B. Wilson, *ACS Nano* **2021**, *15*, 18085–18099.
[27] Y. Chen, N. T. Landes, D. J. Little, R. Beaulac, *J. Am. Chem. Soc.* **2018**, *140*, 10421–10424.
[28] J. De Roo, N. Yazdani, E. Drijvers, A. Lauria, J. Maes, J. S. Owen, I. Van Driessche, M. Niederberger, V. Wood, J. C. Martins, I. Infante, Z. Hens, *Chem. Mater.* **2018**, *30*, 5485–5492.

Manuscript received: May 12, 2022
Accepted manuscript online: May 25, 2022
Version of record online: June 15, 2022